J. Membrane Biol. 122, 215–229 (1991)
002226319100095H

The Journal of
Membrane Biology

Localization of Sodium Absorption and Chloride Secretion in an Intestinal Epithelium

Klavs Holtug†, Al Shipley‡, Vibeke Dantzer§, Ove Sten-Knudsen‖, and Erik Skadhauge§
§Department of Anatomy and Physiology, Royal Veterinary and Agricultural University, Copenhagen; ‡National Vibrating Probe Facility, Marine Biological Laboratory, Woods Hole, Massachusetts; †Department of Medicine A, Rigshospitalet, and ‖Department of General Physiology and Biophysics, The Panum Institute, University of Copenhagen, Copenhagen, Denmark

Summary. Hen coprodeum absorbs sodium electrogenically and, when stimulated by theophylline, secretes chloride. In this study the vibrating microprobe technique was used to localize the transport of these ions to intestinal villi/folds and crypts. With the isolated, stretched epithelium, controlled by light microscopy and scanning electron microscopy, in open circuit, currents were inward, 40 ± 7 $\mu A/cm^2$, 50 μm vertically above villi, and outward, 36 ± 7 $\mu A/cm^2$ above crypts. The currents decayed exponentially to near zero at 300 μm with the same length constant. A physical model simulating the observed loci of current sources and sinks predicts potential profiles consistent with our data. Extrapolation of the currents gives a surface potential of 45 μV, negative on villi and positive above crypts. Short circuiting increased villus current to 86 ± 27 $\mu A/cm^2$ at 50 μm, and amiloride treatment reduced it to −8 $\mu A/cm^2$; in both cases crypt currents were abolished. The inward currents are compatible with sodium absorption. Induction of chloride secretion after amiloride treatment, resulted in current circuits similar to those induced by sodium absorption, with villus currents of 23 ± 7 $\mu A/cm^2$. This is in accord with chloride secretion at the villi. Quantitative estimates of crypt number ($860/cm^2$) and opening diameter (15 μm), in conjunction with isotopic measurements of active and electrical potential-driven ion fluxes demonstrate, however, that only 4% of the potential-driven co-ion transport occurs through the crypts. This indicates that nearly all chloride secretion comes from the sodium-absorbing villar area. Were the chloride secretion to occur solely from the crypts, the current should have been in the opposite direction and 10,000-fold larger.

Key Words intestine · hen · sodium absorption · chloride secretion · villus · crypt · vibrating microprobe · scanning EM

Introduction

Transepithelial ion movement can be divided into transcellular and paracellular transport. During transport of Na^+ from mucosal to serosal solution, in open circuit, movement of this ion is followed by either a negative ion in the same or a positive in the opposite direction. The co-ion movement is thought to be local through the lateral intercellular spaces.

Many epithelia are, however, not a layer of identical cells. They may contain villi and crypts and be composed of different cells. The chloride conductance of amphibian skin has been localized to the mitochondrion-rich cells (Foskett & Ussing, 1986; Katz & Scheffey, 1986; Larsen, 1988). The mitochondrion-rich cell of teleost opercular epithelium secretes chloride actively with virtually no current passing through the adjacent pavement cells (Scheffey, Foskett & Machen, 1983; Foskett & Machen, 1985). The major part of the above results were obtained by local extracellular recording with the vibrating microprobe.

Hen coprodeum is a medium-tight lower intestinal epithelium with villi/folds and crypts. In response to NaCl depletion, electrogenic sodium absorption increases 200-fold (Choshniak, Munck & Skadhauge, 1977) through induction of an amiloride-sensitive sodium channel in the apical membrane (Clauss et al., 1987). Simultaneously a scattered cell population, which could be marked with the silver precipitation technique, appeared on the villi, and coincidentally, chloride secretion could be induced by secretagogues (Clauss, Dantzer & Skadhauge, 1988). Although silver precipitation successfully identified chloride transporting cells in amphibian skin (Willumsen & Larsen, 1986), the technique is indirect and is subject to artifacts. The staining pattern of coprodeum was also incompatible with chloride secretion originating from the crypts as observed by Welsh et al. (1982).

The purpose of this study is to localize sodium and chloride transport in hen coprodeum by the extracellular vibrating microprobe. The results are compatible with sodium absorption and chloride secretion occurring in the same villus cell population. Within the resolution of the microprobe there was no evidence for special transporting cells on villi. The co-ion transport is distributed all over the epithelium with only a minor fraction coming from the crypts.

Materials and Methods

Seven-month-old Cornish hens were used for vibrating microprobe experiments; White Plymouth Rock hens were used for voltage-clamp experiments. They were fed a low-NaCl diet, wheat and barley, and distilled water ad libitum for 14 days prior to experiments (Choshniak et al., 1977). After securing a blood sample for aldosterone analysis (Arnason et al., 1986), the birds were killed by neck dislocation. The lower intestine was quickly removed and the coprodeal epithelium dissected from its muscular layer and placed in 38°C oxygenated Ringer's (mmol/liter: 140 Na, 8 K, 1.3 Ca, 1 Mg, 139 Cl, 1 SO_4, 8 PO_4, and 15 glucose, pH 7.3).

Voltage-Clamp Experiments

The isolated epithelium was mounted in 0.62-cm^2 Ussing chambers and stretched to approximately four times the normal area. The transepithelial potential difference (PD) was monitored with KCl agar bridges and calomel electrodes by a multichannel computer-controlled voltage-clamp unit. The tissues were continuously short circuited at different PDs through Ag/AgCl electrodes (Clauss et al., 1988). An IBM PC computer was connected to the voltage-clamp units and permitted time sharing, on-line control and data acquisition. Tissue resistance was determined by bipolar voltage command steps (usually 5 mV, 300-msec duration). The measurements were corrected for series resistance of the Ringer's between the agar bridges.

Unidirectional fluxes of sodium and chloride were measured with isotopes as described previously (Clauss et al., 1988).

After stabilization of the short-circuit current, the chambers were assigned to be either (*i*) controls with no further additions, (*ii*) amiloride 10^{-4} M added to the mucosal solution, or (*iii*) amiloride 10^{-4} M to the mucosal solution and theophylline 8 mmol/liter to the serosal and mucosal solutions. The epithelia were then clamped in random order to PDs of 45, 30, 15, 0, −15, −30, or −45 mV with respect to the mucosal bath for periods of 30 min for flux determination. The epithelium has previously been shown to be stable for more than 3 hr (Choshniak et al., 1977); the total experimental time was in these experiments 2 hr, allowing flux determinations at three PDs for each tissue.

Vibrating Microprobe Experiments

The isolated epithelium was placed with the serosal side up in a waxed petri dish on parafilm and stretched to four times the area to allow access to the intervillus spaces (*see* Fig. 1). The serosal side was glued along the border to the nylon ring of the perfusion chamber. To stabilize the epithelium the nylon ring was covered with a nylon mesh with a grid size of 250 μm. The tissue was mounted in a horizontal Ussing chamber, with a wide opening at the mucosal top to allow space for the descent of the vibrating microprobe. The serosal and mucosal compartments were perfused separately with 38°C Ringer's solution. The perfusion medium was bubbled with pure O_2. The level of the upper fluid layer was regulated by suction; fluid perfusion of the bottom chamber was regulated by a combination of suction and head pressure to sustain a stable position of the epithelium. The chamber with the epithelium was placed under an upright microscope fitted with Nomarski optics utilizing a Zeiss 40× water immersion objective with a numerical aperture of 0.75 and a working distance 1.7 mm. This allowed continuous video monitoring of the tissue and probe, as well as distance determination, due to the very shallow depth of field (in practice < 3 μm). The epithelial chamber was equipped with a temperature sensor and a pair of KCl agar bridges connected to calomel electrodes. The leads from the current/voltage-clamp units ended in a pair of Ag/AgCl electrodes with the wire leading to the mucosal side being grounded.

For the vibrating probe either platinum or stainless steel electrodes (Micro Probe, Bethesda, MD) insulated with parylene were used. To minimize impedance the uninsulated tip was platinized in a solution of 10 mg/ml H_2PtCl_6 and 100 μg/ml $Pb(CH_3COO)_2$. The stainless steel electrodes were gold plated in 0.2% AuKCN prior to platinization. Final diameter of electrode tips was intended to be 5–10 μm and to have a capacitance of 2–8 nF. The procedure was essentially as described by Jaffe and Nuccitelli (1974). Vibration was accomplished by two piezoelectric reeds vibrating 90° out of phase to make the front of a Lucite rod move in a circular pattern. The probe was connected by a miniature wire pen to the rod front. The excursion movement of the probe tip was 5–10 μm in both vertical and horizontal directions.

The voltage signal from the probe was measured by a differential preamplifier with respect to the platinum-black reference electrode surrounding the mucosal chamber. The signal was sent to a two-phase lock-in amplifier, where the signal was processed with respect to the vibration frequency of the probe in either direction of vibration (Nuccitelli, 1986) to give the potential difference at the peaks of excursion. Calibration of the vibrating probe was done with a known point current source at a 150-μm distance in the directions of vibration, and the voltage signals recorded during experiments were automatically converted to current density. In the experiments the current density became indistinguishable from the background noise at distances more than 300 μm from the epithelium. Consequently, this distance was used for reference measurements.

The experimental protocol was as follows: after establishing reference potential values at 300 μm, the tissue was approached at a distance of 50 μm (occasionally as close as 20 μm) and well-defined villar or crypt regions were scanned. Current density was measured in open circuit and during voltage clamping to PD = 0 mV: current decay with distance from the epithelium was established. These procedures were followed by the addition of amiloride 10^{-4} M, to the mucosal perfusion medium, and the current measurements repeated. Thereafter, theophylline (Sigma), 8 mM, was added to the serosal and mucosal perfusion fluid, and the measurements repeated. During experiments the probe's distance above the epithelium was controlled at approximately 5-min intervals as was the probe's zero output at 300 μm to check for drift in the signal. The waveform of the vibrating probe signal was continuously monitored on an oscilloscope along with the quadrature (i.e., 90° out of phase) output of the lock-in amplifier (Scheffey, 1986) to guard against artifacts.

Histology

Coprodeal tissue from White Plymouth Rock hens was dissected free immediately after slaughter, rinsed and transfered to cold Ringer's solution. Full-wall preparation: a part of the coprodeal wall from a central area of the coprodeum was pinned to a wax plate and fixed in 3% glutaraldehyde in 0.1 mol/liter cacodylate buffer with 2 mmol/liter $CaCl_2$ for 3 hr. Mucosal separation and extension: From a neighboring part the mucosal epithelium was separated at *lamina muscularis mucosae* and used for electrophysiology in the stretched state, or mounted on a nylon ring for $AgNO_3$ treatment and histology.

Silver Nitrate for Light Microscopy

The tissue was incubated in standard Ringer medium oxygenated at 38°C for 30 min. Tissues were rinsed twice in separate baths of near isotonic Na-gluconate solution and afterwards exposed to Na-gluconate with 0.25% $AgNO_3$ for 3 min. After repeated washings in Na-gluconate solution, the tissue was mounted on a microscope slide and exposed to light for 10 min. The epithelium was, later the same day, examined for number of crypts. Details on preparation and examination of "chloride cells" are given by Clauss et al. (1988).

Sections for Light Microscopy

Tissue prepared from the pinned full-wall tissue was stored in the fixative for an additional 1–7 days. The extended stripped epithelium was mounted on the nylon ring and immersed in the fixative. Two- to three-cm long slices were rinsed carefully in buffer, dehydrated and embedded by routine methods in Histo-Resin (LKB). Sections, 1–3 μm thick, were stained with conventional stains: toluidine blue, hematoxylin eosin or Giemsa. The measurements were made with an Olympus AH2 light microscope using a side entry measuring graticule.

Scanning Electron Microscopy (EM)

An area of 0.5 × 0.5 cm^2 epithelium was stored in the fixative for 1–7 days. The tissue was rinsed in the same buffer as used for the fixative before being dehydrated in graded series of acetone and critically freeze-dried in a Balzer critical point dryer. Subsequently, the specimens were mounted on copper carriers and sputter coated with 20-nm gold in a Polaron high resolution sputter coater, before examination in a Jeol JSM T20 or JSM 840 A at 15 kV.

Statistical Analysis

Results are expressed as mean ± SEM, with (n) denoting the number of experiments. Curves were fitted by linear-regression analysis or nonlinear regression to produce optimum fits as evaluated by the chi-square value. The reciprocal of SD was used as weight in fitting procedures.

Results

Morphology

Light microscopy revealed a mucosal membrane with short and broad villi or irregular folds with short intestinal glands (Liberkühn's crypts). The intestinal glands became even more distinct in the stretched mucosal preparations (Fig. 1). The crypt length varied from 50 to 130 μm (mean 80 μm), measured on both the full-wall preparations and on the stretched mucosa. In the stretched epithelium, the villi were flattened, and the mucosal surface area was estimated to be 1.5 to 2 times the serosal area.

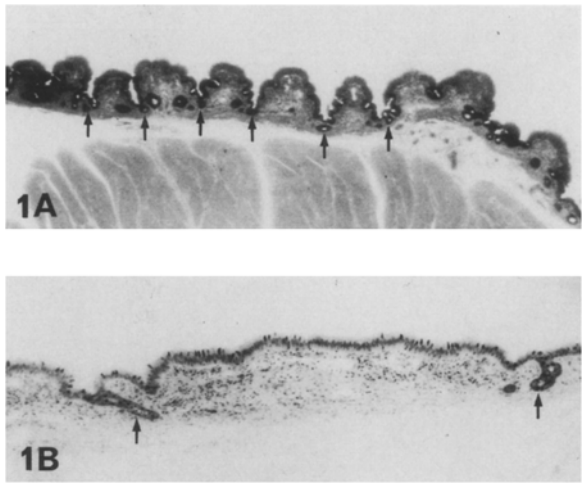

Fig. 1. Light micrographs of the coprodeal wall. (*A*) Section of pinned whole-wall preparation with the tunica mucosa, tela submucosa and some parts of tunica muscularis. Notice the formation of high broad "villi" (*compare* to Fig. 2) and the short crypts (arrows) between them. Magnification 23 ×. (*B*) Tunica mucosa of coprodeum fixed, as stretched for microprobe electrophysiology. Notice the crypts (arrows), and the relative smooth surface. Magnification 43 ×

The scanning EM demonstrated the "villi" of the coprodeum to be low irregular folds separated by furrows (Figs. 2 and 4). On the stretched mucosa the furrows between the folds can be clearly visualized (Figs. 3, 5 and 6), and thereby, the openings of the crypts (Figs. 5 and 6). The epithelium have goblet cells, seen as small holes at higher magnifications (Figs. 4 and 5).

The dark precipitates in the stretched mucosa treated with $AgNO_3$ show the so-called "chloride cells" and also an affinity for the crypt openings (Fig. 7), which demonstrate their great variation in diameter (Figs. 6 and 7). Circular crypts were clearly visible and were often found along the midline of the furrows between the ridges with an intercrypt distance of approximately 100 μm. (Crypts could also be identified at the unstained tissue by light microscopy and by the Nomarski technique during the probe experiments.) The crypts were counted in 20 circular fields of 1.63 mm^2 from the Ag-stained coprodeum of a low-NaCl hen. The number ranged from 0–31 per field with an average 8.6 ± 1.2 crypts per mm^2, or 860 per cm^2. The crypt diameter measured on the $AgNO_3$-treated specimens varied from 4 to 35 μm with most of the openings from 10 to 20 μm. The fractional area of the crypts can be estimated to be approx. 2% of the stretched (flat) area of the epithelium.

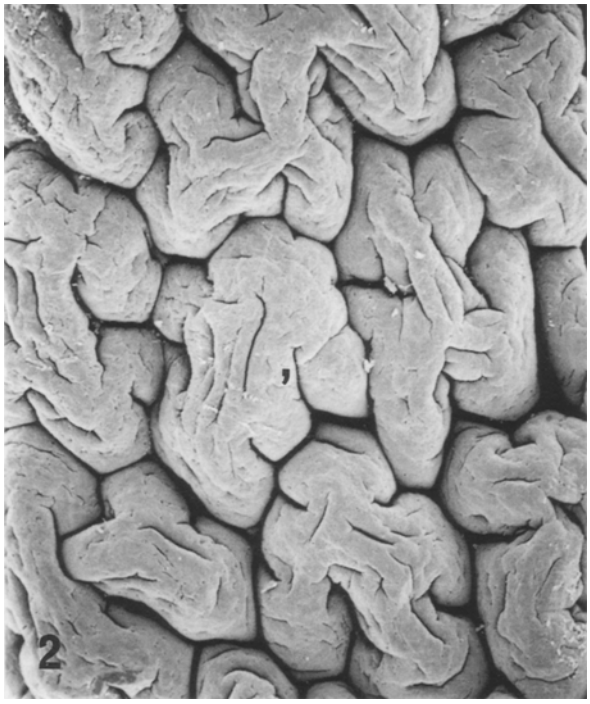

Fig. 2. Scanning electron micrograph from pinned wall of the coprodeum showing the elongated folds. The bottom of the furrows between the folds, where the crypts open, cannot be seen. Magnification 50×

Fig. 3. Scanning electron micrograph of coprodeum after "stripping" and mounting stretched in the Ussing chamber, as for microprobe measurements. Fixing was performed in the chamber. Notice the extended mucosal folds (*F*) and the visible fossae (*). Magnification 49×

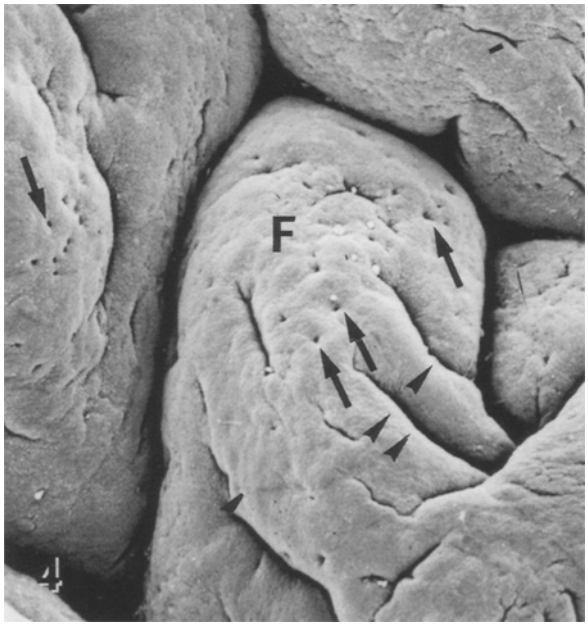

Fig. 4. Scanning electron micrograph of coprodeal pinned specimen. The mucosal folds (*F*) have small irregular furrows (arrowheads); the base of the folds and the openings of the crypts cannot be seen. The small holes represent goblet cells (arrows). Magnification 210×

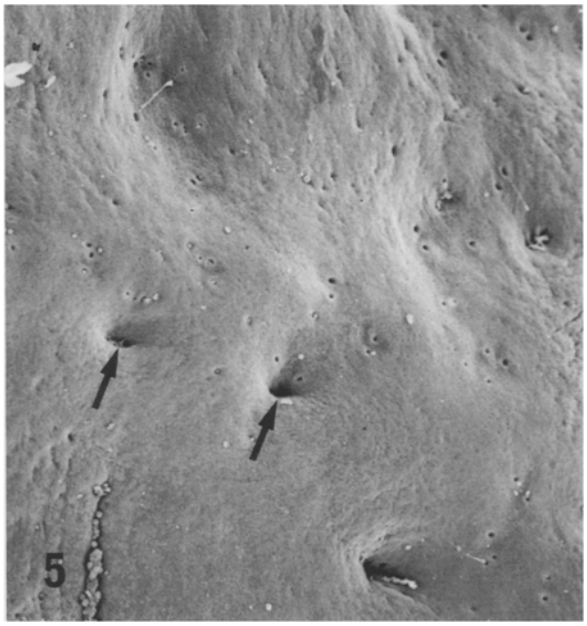

Fig. 5. Scanning electron micrograph of stretched coprodeal mucosa showing the base of mucosal folds and bottom of the fossae with openings of the crypts (arrows). The small holes represent openings of goblet cells. Magnification 100×

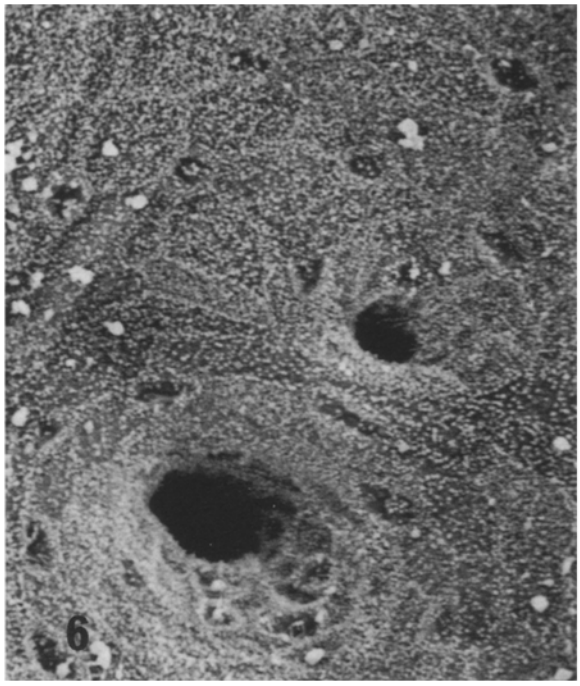

Fig. 6. Scanning electron micrograph of detail of crypt openings in the bottom of a fossa. The lining of the individual cells can be discerned in some cases. Magnification 2300×

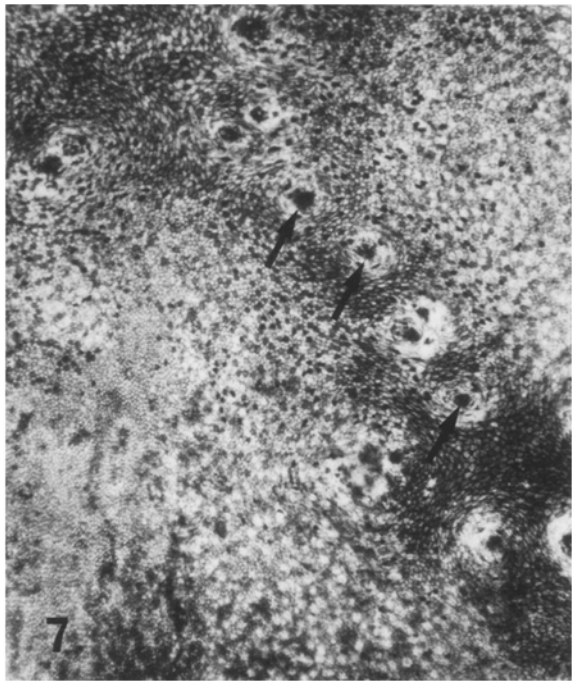

Fig. 7. Light micrograph of whole mucosal membrane treated with $AgNO_3$, demonstrating precipitates of AgCl at the crypt openings (arrows). The "chloride cells" are only discernable as fine dark spots. Magnification 136×

Table 1. Electrical parameters of Cornish hen coprodeum in an Ussing chamber, before and after sequential addition of amiloride, theophylline, and bumetanide (mean ± SEM (n))

	I_{sc} (μA/cm^2)	PD (mV)	Resistance (Ω cm^2)
Control	159 ± 12 (10)	−24 ± 3 (10)	160 ± 24 (10)
Amiloride	−3.2 ± 4.0 (10)	0.3 ± 1.1 (10)	238 ± 33 (10)
Theophylline	73.5 ± 11 (10)	−9.7 ± 1.2 (10)	132 ± 17 (10)
Bumetanide	16.9 ± 3.7 (9)	−2.8 ± 0.9 (9)	207 ± 85 (9)

I_{sc}, short-circuit current; PD, electrical potential difference.

Comparison of Cornish and Plymouth Rock Hens

Voltage-clamp experiments on Cornish hens are reported in Table 1. The epithelium was in these experiments treated conventionally and not stretched as in the other experiments. The current was inhibitable by amiloride. Stimulation with theophylline produced an increase in current, which partly was inhibited by bumetanide. These responses are similar to those of Plymouth Rock hens (Clauss et al., 1988).

Plasma aldosterone of the Cornish hens was 181 ± 27 pg/ml (n = 21), very similar to values in Plymouth Rock hens (Arnason et al., 1986; Clauss et al., 1988) on the same dietary scheme.

Ion Flux Dependence on Transepithelial Potential Difference

The transepithelial current-voltage relationship is depicted in Fig. 8. There was a difference in current at any voltage depending on whether tissues were controls, treated with amiloride, or with amiloride and theophylline. The stretched tissues clamped to 0 mV had short-circuit currents reduced by a factor of 2–3 compared to unstretched tissues (Clauss et

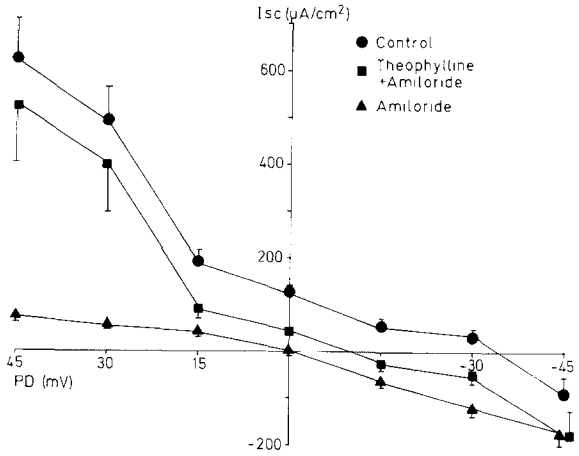

Fig. 8. Current response to voltage clamping in hen coprodeum to different PDs. Tissues were either control, pretreated with mucosal 0.1 mM amiloride, or 0.1 mM amiloride and 8 mM theophylline on both sides. Points are means of 12–24 individual measurements

dium mucosa-to-serosa fluxes are in the presence of mucosal amiloride indistinguishable from the serosa-to-mucosa fluxes. Under control conditions, there was a large net sodium absorption also linearly dependent on the electrical driving force.

Figure 10 illustrates the dependence of the unidirectional chloride fluxes on transepithelial electrical PD. Chloride mucosa-to-serosa fluxes were identical, independent of amiloride and theophylline, and linearly dependent on the electrical driving force. Theophylline increased chloride serosa-to-mucosa flux at negative potentials. As transepithelial potentials became positive a chloride serosa-to-mucosa conductance was activated, except in experiments with only amiloride added. The potential-activated chloride conductance was identical in control tissues and epithelia pretreated with theophylline.

Vibrating Microprobe Experiments

Due to the mucus layer above the mucosal surface of the epithelium, the closest working distance of

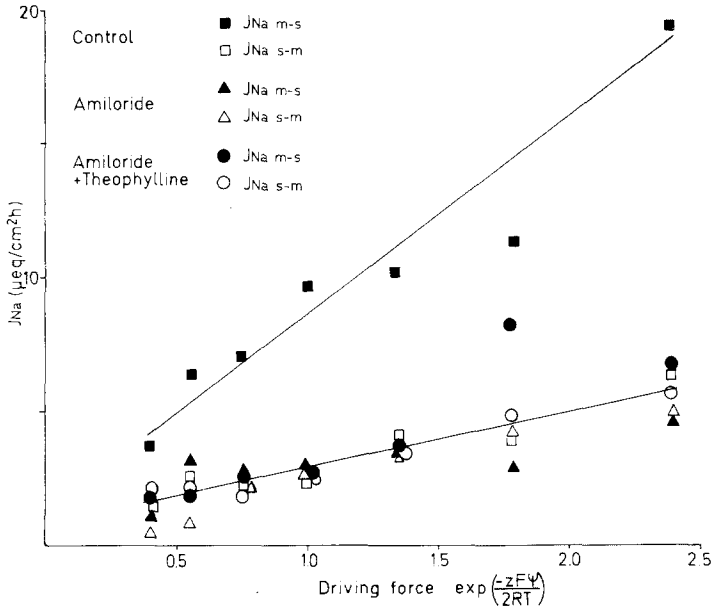

Fig. 9. Unidirectional sodium fluxes depending on the electrical driving force. The tissues were pretreated as in Fig. 8. Points are means of 6–12 determinations. *m-s*, mucosa to serosa; *s-m*, serosa to mucosa; *F*, Faraday's constant; *R*, gas constant; *z*, charge number of ion; *T*, absolute temperature; and ψ, electrical potential of the *trans* compartment when the *cis* compartment has an electrical potential of zero

al., 1988), reflecting the reduced amount of transporting epithelium. The open-circuit electrical PD, where the transepithelial current is zero, can be obtained from Fig. 8 and corresponds to open-circuit values of unstretched tissue (33 *versus* 37 mV; Choshniak et al., 1977).

Sodium fluxes in response to transepithelial PD, amiloride, and theophylline are shown in Fig. 9. Sodium serosa-to-mucosa fluxes were linearly dependent on the electrical driving force and independent of amiloride and theophylline treatment. So-

the vibrating probe for repeated measurements was 50 μm. At this distance differences in single cell currents cannot be recorded; even in the few experiments where it was possible to approach the epithelium down to 11 μm, it was impossible to detect any difference in current over individual cells. In a series of initial experiments performed with the probe vibrating in one direction 20 μm above the tissue, it was not possible to distinguish cells with different currents.

With the epithelium in open circuit, no change

Table 2. Vibrating probe measurements of currents 50 μm above the isolated hen coprodeum[a]

	I_{sc} $\mu A/cm^2$	Villus		Crypt	
		I_{vp_s} $\mu A/cm^2$	I_{vp_0} $\mu A/cm^2$	I_{vp_s} $\mu A/cm^2$	I_{vp_0} $\mu A/cm^2$
Control	91 ± 16 (10)	40 ± 7 (12)	86 ± 27 (10)	−36 ± 7 (12)	9 ± 4 (8)
Amiloride		−8 ± 4 (10)		−15 ± 4 (12)	
Amiloride + Theophylline		23 ± 7 (6)		−12 ± 3 (4)	

[a] The results were obtained above villi and crypts during open and short circuit; conventional short-circuit current is likewise given. The measurements were performed during control conditions with 0.1 mM amiloride in the mucosal solution and with further addition of 8 mM theophylline to the serosal and mucosal solution. Values are mean ± SEM (number of tissues); I_{vp_s} were estimated at 5–10 sites in each tissue.

I_{sc}, short-circuit current; I_{vp}, current measured with the vibrating probe; $_s$, during open-circuit/spontaneous PD; $_0$, with tissue voltage clamped to 0 mV. Current direction into the epithelium defined as positive.

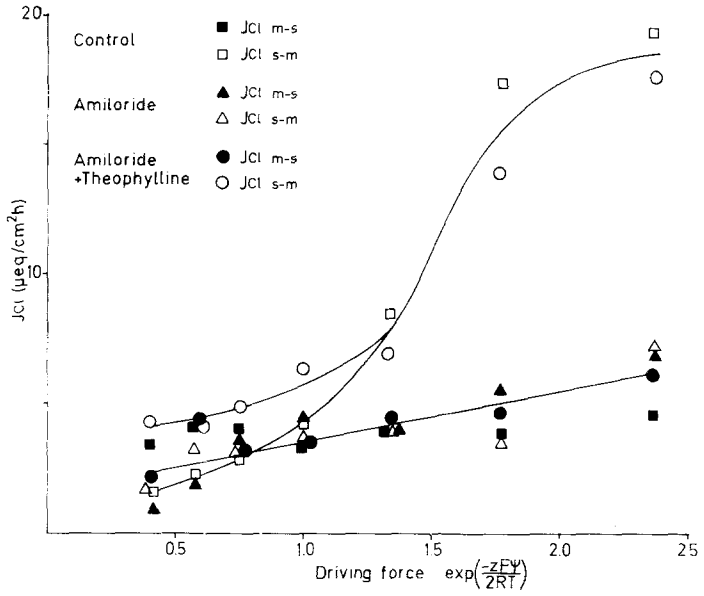

Fig. 10. Unidirectional chloride fluxes in response to voltage clamping to different electrical driving forces. The epithelia were pretreated as in Fig. 8. Individual points are means of 6–12 determinations. *m-s*, mucosa to serosa; *s-m*, serosa-to-mucosa; *F*, Faraday's constant; *R*, gas constant; *z*, charge number of ion; *T*, absolute temperature; and ψ, electrical potential of the *trans* compartment with respect to the *cis* compartment

in current was detected more than 300 μm away from the tissue, so this position was chosen for reference. When the probe was positioned 50 μm above the more central part of a villus, an inward current (positive current into the epithelium) was always observed (Table 2). Positioned in the intervillous space above a crypt, the probe measured an outward current (positive current out of the epithelium or negative current into the epithelium) (Table 2).

The large currents 50 μm above villi and crypts were followed to the chosen reference 300 μm by increasing the probe/tissue distance in steps of 25–50 μm. The dependence of the luminal current density on the perpendicular distance from the surface of either the villi or the crypts is shown in Fig. 11. A positive value of the current density implies an inward direction of the current, i.e., directed from the lumen to the epithelial surface. The configuration of the decay suggested that the data were fitted to an exponential function of the form:

$$I(x) = I_0 \exp(-x/\lambda) \quad (1)$$

where $I(x)$ is the current density at a distance x from

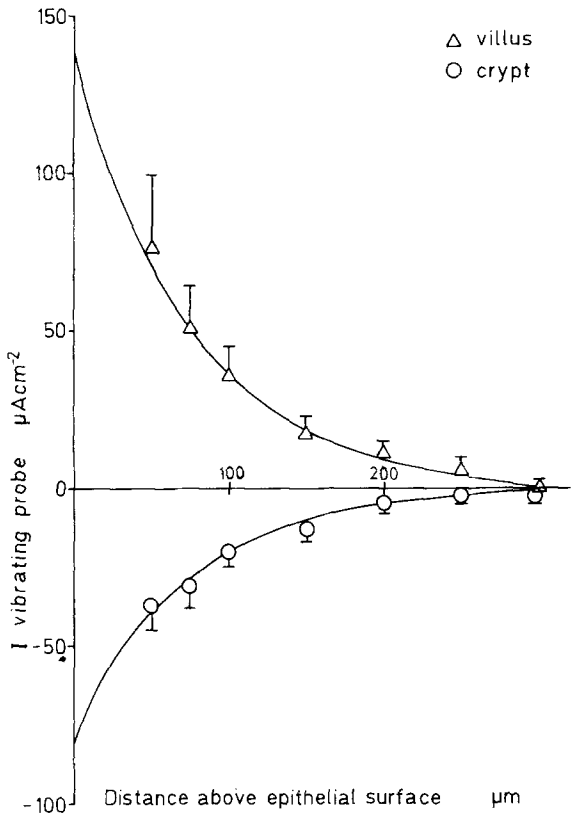

Fig. 11. Current measurements obtained with the vibrating microprobe at different distances above villi and crypts in hen coprodeum. Values are means ± SEM of 10 tissues. Lines are from results of least-squares nonlinear regression analysis to exponential decay

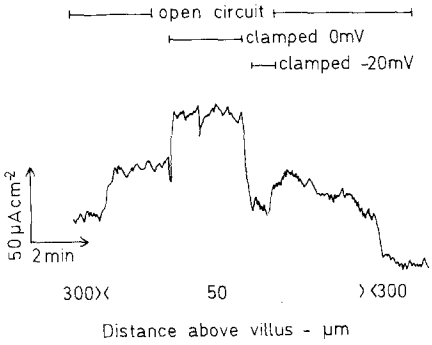

Fig. 12. Original vibrating microprobe recording above a villus. Only the dimension vertical to the epithelium was recorded. Distance 300 μm above the epithelium was reference; moving the probe to 50 μm reveals an inward current at a spontaneous PD of −11 mV. Voltage clamping the tissue to 0 mV increases the inward current; voltage clamping to −20 mV decreases the current

the epithelium, I_0 represents the current density at the surfaces of the crypts and villi, and λ is a length constant for the exponential decay. A least-square nonlinear regression resulted in the following values for these two parameters:

$$I_0\ (\mu A/cm^2) = \begin{cases} \text{Villi: } 140 \pm 19 \\ \text{Crypt: } -80 \pm 9 \end{cases}$$

and

$$\lambda(\mu m) = \begin{cases} \text{Villi: } 73.5 \pm 6.0 \\ \text{Crypt: } 73.0 \pm 5.3. \end{cases} \quad (2)$$

Thus, the length constants for the current decay were identical above villi and crypts.

To calculate the surface electrical potential of crypts and villi from the current density data above, we invoke the following form of Ohm's law: $d\psi(x)/dx = -\rho I(x)$, where $\psi(x)$ and $I(x)$ are the electrical potential and current density both at the position x in the lumen measured along the normal to the epithelial surface and ρ is the resistivity of the luminal content ($\Omega \cdot$ cm). We insert Eq. (1) into the above form of Ohm's law (with the conventions as to the sign of the current density taken into account) and integrate it from $x = \infty$, where $\psi(\infty) = 0$, to $x = 0$ where $\psi(0) = \psi_s$. This gives

$$\int_0^{\psi_s} d\psi = \psi_s = \rho I_0 \int_{\infty}^{0} \exp(-x/\lambda) dx = -\lambda \rho I_0. \quad (3)$$

Using the above values from villi gives a surface potential

$$\psi_s^{\text{villi}} = -73.5 \cdot 10^{-4}\,\text{cm} \cdot (-140\,\mu\text{A} \cdot \text{cm}^{-2}) \cdot 56.3\ \Omega \cdot \text{cm} = -58\ \mu\text{V},$$

whereas average numeric values (crypt and villus) gives 45 μV.

Short-circuiting to 0 mV PD had different effects on vibrating probe measurements above villi and crypts (Table 2). An illustration with the probe above a villus is shown in Fig. 12, which shows that the inward current increased. Voltage clamping to −20 mV, which was above the spontaneous PD, decreased current above the villi. The outward current above the crypts was abolished during short circuiting to 0 mV (Fig. 13). Increasing the clamp PD to −20 mV, which was above the open-circuit PD, increased the outward current above the open-circuit value.

Inhibition of the apical sodium channel by 0.1 mM amiloride at the mucosal surface decreased the current above the villi to the reference values within 2 min. The same effect was observed on the crypt current (Table 2). The small currents measured after

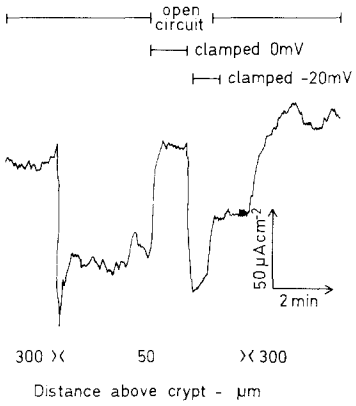

Fig. 13. Vibrating probe recordings above a crypt. Reference distance was 300 μm above epithelial surface. Bringing the probe down to 50 μm above the tissue records a negative (outward) current, which disappeared with voltage clamping to 0 mV

amiloride may, apart from background error, be due to proton and/or potassium secretion. Stimulation of chloride secretion by theophylline produced an increase of the inward current on villi (Table 2), but with no change in crypt outward current.

Discussion

Sodium and Chloride Fluxes

The stretched coprodeum responded in the Ussing chamber qualitatively similar to the conventionally mounted epithelium (Clauss et al., 1988). The magnitude of currents, sodium absorption, and chloride secretion was reduced, presumably due to the decrease in absolute number of transporting cells (apical area). Passive fluxes were unchanged. This may be because decreased diffusion resistance in intervillar space and reduced total mucosal area cancel out (Harris & Kennedy, 1988; Holzheimer & Winne, 1989). Stretching the coprodeum is not unphysiological, but part of its normal storage function (Skadhauge, 1981).

The results were otherwise compatible with previous findings, i.e., apical amiloride-sensitive sodium and theophylline-activated chloride channels (Choshniak et al., 1977; Clauss et al., 1988).

After amiloride addition to the mucosal bath, sodium mucosa-to-serosa and serosa-to-mucosa fluxes were equal and showed identical dependence on the electrical driving force. The path thus has identical permeability in either direction. This favors an extracellular shunt (Frizzell & Schultz, 1972). Mucosa-to-serosa chloride fluxes were independent of amiloride and theophylline and had permeabilities very close to those of sodium. After amiloride, chloride fluxes showed the same serosa-to-mucosa permeability, and PD dependence, as for sodium, suggesting a paracellular path for these fluxes.

Transepithelial PD depended in open circuit entirely on net sodium absorption and was decreased compared to the short-circuited state. Mucosa-to-serosa chloride flux increased, while serosa-to-mucosa flux decreased; there was also an increased flux of sodium serosa to mucosa. The sum was electroneutral NaCl absorption. After amiloride and theophylline, active transport was chloride secretion and the created PD in open circuit balanced paracellular transport, so the sum was NaCl secretion.

Vibrating Microprobe Experiments

To determine the electric field arising from the individual cells it was required to scan with the microprobe at a distance of 10–20 μm above the tissue. Technically this turned out to be very difficult. The successful attempts of scanning the cell surface horizontally at this distance showed no change in local currents. However, we observed large currents above the epithelium with distinct and consistent differences between anatomic structures. These currents decayed with the distance from the mucosa and became indistinguishable from the background noise at a distance of 300 μm above the mucosa.

Inward currents, i.e., positive currents directed from the lumen towards the mucosal surface, were observed above the villi and outward currents in the crypt/intervillous area. The decay of the currents measured along the normal to these two regions fitted well to exponential decay; furthermore, the decay in the two regions were characterized by the same length constant $\lambda = 73$ μm, i.e., the distance where the current has decayed to 0.37 of the value at the surface (Fig. 11). From the decay in current density with distance from the mucosal surface and the solution resistivity determined to 56.3 $\Omega \cdot$ cm, the calculated surface potential was (on average) 45 μV negative on villi and 45 μV positive at the crypts, which suggests the presence of a volume flow of current in the luminal field which arises at the crypts and terminates on the villi.

To substantiate this idea it was considered of interest to examine whether the extent into the lumen of the observed current flow and the shape of its decay could be simulated by a simple physical model with electrical properties analogous to those present at the mucosal surface. The electrical data taken together with the structural organization suggest a model consisting of a large set of parallel coplanar strips of sources and sinks charged alter-

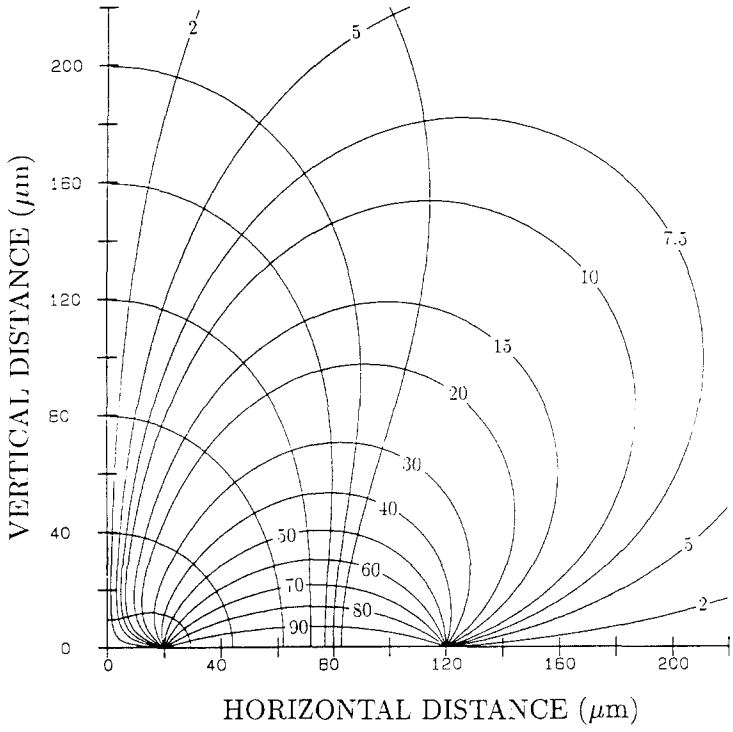

Fig. 14. Model calculations, Appendix Eqs. (A7) and (A14): Equipotential lines and current lines in the upper right half when the strip between 20 and 120 μm is charged to the potential $U_0 = 100$, and a similar strip in the left-half plane between -20 and -120 μm is charged to $U_0 = -100$. Abscissa: Distance (μm) measured horizontally along the epithelium from the midpoint between the strips. Ordinate: Distance (μm) measured along the normal to the epithelial surface. The closed set of curves originating from the two sides of the strip are the equipotentials with their appropriate value being indicated by the number on the line. The current lines (which indicate the direction of the current at the position in question in space) diverge from the strip and end symmetrically oriented with respect to the y-axis on the negatively charged strip

natingly to $+45$ and -45 μV. The mutual distances in the arrangement of sources (crypts) and sinks (villi) were chosen to be similar to those of the tissue. In the Appendix are given the details of the calculation of the equipotential profiles, current lines and current densities which the model generates. An example of equipotential profiles and current lines in the right hand half-plane is presented in Fig. 14. The decay of current and potential along the normal directed from the center of the source/sink region is nearly exponential, and the shape is closely similar to that obtained from the experimental data. The distance from the source at which the potential has decayed to less than 1% of the surface value is about 300 μm (Fig. 15) and agrees well with the distance from the epithelial surface chosen as the reference distance. As expected the highest current densities are those arising from the edge of the positively charged strip and running almost horizontally to the adjacent edge of the negatively charged strip. Furthermore, Fig. 14 also shows that the horizontal region, inside which the potential and the direction of the field lines changes relatively little, spreads out with increasing distance from the midregion of the strip. This behavior was also observed experimentally when the vibrating microprobe was moved horizontally at various distances from the mucosal surface. As a further test the vertical current densities $I_y(x,y)$ which the model would predict were calcu-

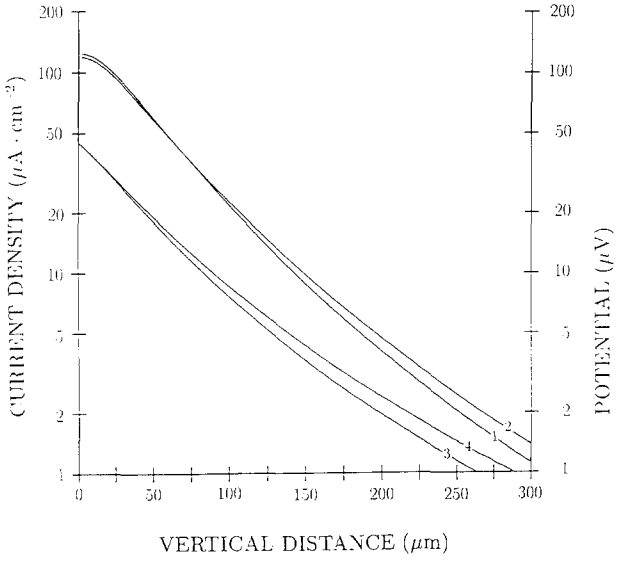

Fig. 15. Model calculations, Appendix Eqs. (A7) and (A16): Semilogarithmic plot of calculated current densities along the normals to the strip placed at positions $x = 60$ μm (curve 1) and $x = 80$ μm (curve 2) and the corresponding potential profiles (curves 3 and 4), using the average value obtained for the surface potential $U_0 = 45$ μV and the resistivity $\rho = 56$ $\Omega \cdot$ cm of the Ringer's fluid actually used

Table 3. Unidirectional fluxes in open circuit[a]

PD (mV)	Control −33	+Amiloride 0	+Theophylline −12
Fluxes (μeq/cm^2 hr)			
J_{Na} *m-s* active	4.0	0	0
paracell	2.0	2.5	2.0
J_{Na} *s-m* active	0	0	0
paracell	4.0	2.5	3.0
J_{Cl} *m-s* active	0	0	0
paracell	4.5	4.0	4.0
J_{Cl} *s-m* active	0	0	2.0
paracell	2.5	4.0	3.0

[a] The results were obtained from Figs. 8–10. The passive fluxes were taken from tissues treated with amiloride at the appropriate PD and were subtracted from total fluxes to obtain the active flux. Values were rounded to nearest 0.5 μeq/cm^2 hr.
m-s, mucosa to serosa; *s-m*, serosa to mucosa.

lated by inserting into Eq. (A16) of the appendix the average value for the surface potential $U_0 = 45\ \mu V$ and the value $\rho = 56\ \Omega \cdot$ cm for the resistivity of luminal Ringer's solution. Figure 15 shows two examples of current densities $I_y(x,y)$ as functions of the vertical distance y from the (x,z)-plane calculated at the positions $x = 60\ \mu m$ and $x = 80\ \mu m$. The current densities decline almost exponentially with distance y to 1–2% of the surface value at a distance of about 300 μm. Furthermore, the model predicts values of the current densities at the surface $y = 0$ to be in the range of 100–150 $\mu A \cdot cm^{-2}$ values which agree well with those predicted by extrapolation of the experimentally measured current densities. Thus, the predictions from the theoretical model support the view that regions of the crypts and villi are the sources and sinks for current flow observed in the luminal fluid.

The nature of this current circuit was then to be determined. A net absorption of sodium ions should be recorded as an inward current. Since such a current actually was observed, sodium absorption on the villi (folds) became highly plausible. To substantiate it, probe measurements were performed under short circuiting. This doubled the villus inward current, as expected if this was caused by sodium transport (Fig. 12, Table 2). The crypt current was abolished with short circuiting. It must therefore represent the co-ion transport, which in open circuit is driven by the PD. The ions responsible for this outward current would be chloride mucosa-to-serosa and sodium serosa-to-mucosa. In a further attempt to characterize the currents, amiloride was added to inhibit the apical sodium channel. All currents were inhibited within 2 min, as expected. The villus inward current is thus beyond reasonable doubt caused by sodium absorption. Addition of theophylline elicits chloride secretion. In the tissues where measurements were technically possible, inward currents reappeared at the villi. This supports several recent suggestions that in some gastrointestinal epithelia, chloride secretion originates from the villi (De Jonge, 1975; Giraldez, Sepulveda & Sheppard, 1988; Diener et al., 1989; Stewart & Turnberg, 1989).

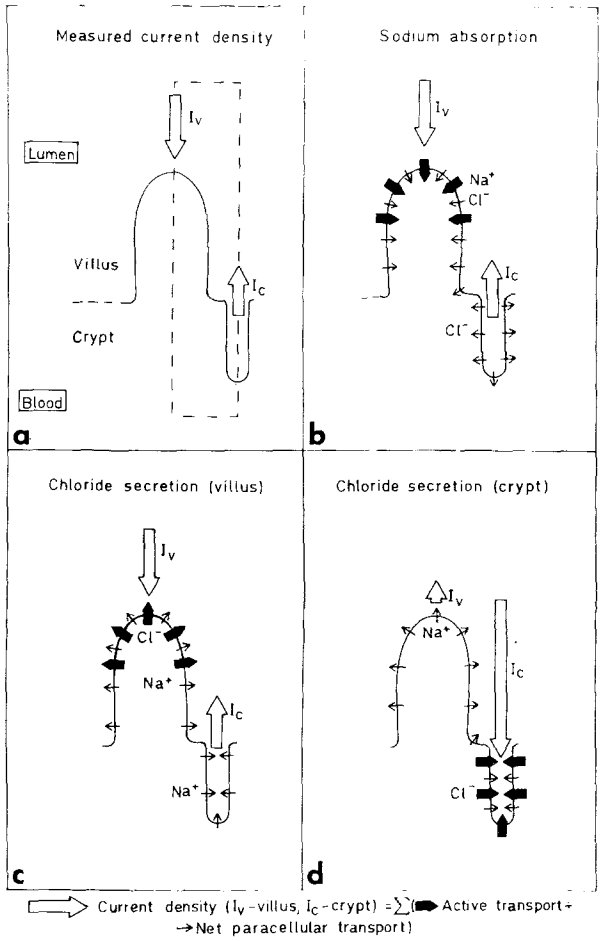

Fig. 16. Interpretation of measured current densities. (*a*) shows the measured current densities above villi (folds) and crypts. (*b*) Shows the villus inward current interpreted as Na absorption with the outward crypt current interpreted as net inward migration of Cl (in open circuit). (*c*) Shows interpretation of inward villus current after amiloride-theophylline as Cl secretion with outward crypt current interpreted as net Na migration in the outward direction. (*d*) Shows the consequence of measured Cl secretion postulated to occur solely from the crypts: the current would have to be in the opposite direction of that observed and 10,000-fold larger

Table 4. Calculated estimates of extracellular currents based on different models of sodium absorption and chloride secretion, *see below*[a]

$\mu A/cm^2$	Measured	I	II	III	IV
Control					
Villus	80	73	71		142
Crypt	−72	−1512	−293		−47035
Amiloride					
Villus	−16	0	0	0	0
Crypt	−30	0	0	0	0
Theophylline					
Villus	46	35	35	−35	71
Crypt	−24	−757	−73	11×10^5	-11×10^5

[a] For comparative purposes, the measured values from Table 3 are extrapolated to the epithelial surface given in the column "Measured." The currents present after addition of amiloride may be accounted for by proton and potassium secretion.
Model I: Uniform paracellular pathway; active transport localized to villi (50% of total tissue area). Model II: Opening diameter of crypt increased to 60 μm. Model III: All chloride secretion occurring in crypts. Model IV: Active transport occurring on villi; all passive transport in crypts.

Synthesis

Our data can be combined to determine their agreement with the possible organization of active and passive transport. The histological data allow determination of approximate mucosal surface area (1.5 cm^2 per cm^2 serosal area), total crypt area (2π (7.5 μm) · (80 μm) · (860) = 0.03 cm^2 per cm^2 serosal surface), and crypt opening area (π (7.5 $\mu m)^2$ (860) = 0.0015 cm^2). The open-circuit fluxes can be estimated from their dependence on transmucosal PD. They are shown in Table 3. The passive paracellular fluxes can be determined from the fluxes after amiloride treatment at the appropriate transmucosal PD. From these transport rates the expected current values at the epithelial surface can be calculated, making different assumptions about the localization of the pathways for active and passive transport (Table 4 and Fig. 16).

Model I had all active sodium absorption localized to 50% of the villus area and the paracellular/passive transport distributed evenly across the epithelium. The sodium absorption corresponds well with the measured value. The crypt current is underestimated. The most obvious reason for this is the sensitivity of calculated crypt current to the crypt area and especially crypt opening diameter which both are prone to error. Also, since the vibrating probe experiments were performed under visual guidance the largest crypts were probably selected. In model I chloride secretion is supposed to occur from the same area and cell population as sodium absorption. The model and the experimental results are in exact agreement.

If, on the contrary, the conventional hypothesis (model III) that chloride secretion were to occur from the crypts, the predicted crypt currents would be in the opposite direction and 10,000-fold larger than those measured.

Conclusion

Hen coprodeum absorbs sodium actively by an amiloride-sensitive mechanism located at the cells on the villi (folds). Chloride is secreted after stimulation with theophylline. Secretion occurs from the same area/cells as active sodium absorption. The paracellular path for ion transport seems to be evenly distributed over the epithelium. Due to the large proportion of surface area localized to the crypts relative to their opening area, the epithelium exhibits current circuits between villi and crypts. These are responsible for 4% of the epithelial transport.

This study was supported by the Danish Natural Science Research Council and NATO grant 118/82. Equipment was donated by Velux (1981) Foundation and the NOVO Foundation. We thank Bente Schousboe and Inge Bjerring Nielsen for superb technical assistance and the staff at MBL, particularly Steve Dixon, for the hospitality and excellent working conditions.

We especially thank Dr. Lionel Jaffe, MBL, who made a very central contribution to our interpretation, apart from making it all possible.

References

Arnason, S.S., Rice, G.E., Chadwick, A., Skadhauge, E. 1986. Plasma levels of arginine vasotocin, prolactin, aldosterone and

corticosterone during prolonged dehydration in the domestic fowl: Effect of dietary NaCl. *J. Comp. Physiol.* **156:**383–397
Choshniak, I., Munck, B.G., Skadhauge, E. 1977. Sodium chloride transport across the chicken coprodeum. Basic characteristics and dependence on sodium chloride intake. *J. Physiol.* **271:**489–504
Churchill, R.V. 1960. Complex Variables and Applications. pp. 242–258. McGraw-Hill, New York.
Clauss, W., Dantzer, V., Skadhauge, E. 1988. A low-salt diet facilitates Cl secretion in hen lower intestine. *J. Membrane Biol.* **102:**83–96
Clauss, W., Dürr, J.E., Guth, D., Skadhauge, E. 1987. Effects of adrenal steroids on Na transport in the lower intestine (Coprodeum) of the hen. *J. Membrane Biol.* **96:**141–152
De Jonge, H.R. 1975. The response of small intestinal villous and crypt epithelium to cholera toxin in rat and guinea pigs. Evidence against a specific role of the crypt cells in choleragen-induced secretion. *Biochim. Biophys. Acta* **381:**128–143
Diener, M., Rummel, W., Mestres, P., Lindemann, B. 1989. Single chloride channels in colon mucosa and isolated colonic enterocytes of the rat. *J. Membrane Biol.* **108:**21–30
Foskett, J.K., Machen, T.E. 1985. Vibrating probe analysis of teleost opercular epithelium: Correlation between active transport and leak pathways of individual chloride cells. *J. Membrane Biol.* **85:**25–35
Foskett, J.K., Ussing, H.H. 1986. Localization of chloride conductance to mitochondria-rich cells in frog skin epithelium. *J. Membrane Biol.* **91:**251–258
Frizzell, R.A., Schultz, S.G. 1972. Ionic conductances of extracellular shunt pathway in rabbit ileum: Influence of shunt on transmural sodium transport and electrical differences. *J. Gen. Physiol.* **59:**318–346
Giraldez, F., Sepulveda, F.V., Sheppard, D.N. 1988. A chloride conductance activated by adenosine 3′,5′-cyclic monophosphate in apical membranes of *Necturus* enterocytes. *J. Physiol.* **395:**597–623
Harris, M.S., Kennedy, J.G. 1988. Relationship between distention and absorption in rat intestine: II. Effects of volume and flow rate on transport. *Gastroenterology* **94:**1172–1179
Holzheimer, G., Winne, D. 1989. Influence of distension on absorption and villous structure in rat jejunum. *Am. J. Physiol.* **256:**G188–G197
Jaffe, L.F., Nuccitelli, R. 1974. An ultrasensitive vibrating probe for measuring steady extracellular currents. *J. Cell. Biol.* **63:**614–628
Katz, U., Scheffey, C. 1986. The voltage-dependent chloride current conductance of toad skin is localized to mitochondria-rich cells. *Biochim. Biophys. Acta* **861:**480–482
Larsen, E.H. 1988. NaCl transport in a high resistance epithelium: The amphibian skin. *In:* Advances in Comparative and Environmetal Physiology. Vol. 1, pp. 189–248. R. Greger, editor. Springer-Verlag, Berlin
Morse, P.M., Feshbach, H. 1953. Methods of Theoretical Physics. Part I, pp. 370–373. McGraw-Hill, New York
Nuccitelli, R. 1986. A two-dimensional vibrating probe with a computerized graphics display. *In:* Ionic currents in development. Progress in Clinical and Biological Research. Vol. 210, pp. 13–20. Alan R Liss, Somerset (NJ)
Scheffey, C. 1986. Pitfalls of the vibrating probe technique, and what to do about them. *In:* Ionic Currents in Development. Progress in Clinical and Biological Research. Vol. 210, pp. 3–12. Alan R. Liss, Somerset (NJ)
Scheffey, C., Foskett, J.K., Machen, T.E. 1983. Localization of ionic pathways in the teleost opercular membrane by extracellular recording with a vibrating probe. *J. Membrane Biol.* **75:**193–203
Skadhauge, E. 1981. Osmoregulation in birds. Springer-Verlag, Berlin
Stewart, C.P., Turnberg, L.A. 1989. A microelectrode study of responses to secretagogues by epithelial cells on villus and crypt of rat small intestine. *Am. J. Physiol.* **257:**G334–G343
Welsh, M.J., Smith, P.L., Fromm, M., Frizzell, R.A. 1982. Crypts are the site of intestinal fluid and electrolyte secretion.*Science* **218:**1219–1221
Willumsen, N.J., Larsen, E.H. 1986. Membrane potentials and intracellular Cl^- activity of toad skin epithelium in relation to activation and deactivation of the transepithelial Cl^- conductance. *J. Membrane Biol.* **94:**173–190

Received 18 September 1990; revised 25 January 1991

Appendix

An Electrostatic Analogue

The aim of the analysis presented is to examine whether the potential and current profiles observed in the luminal fluid by means of the vibrating electrode can be accounted for by a simple electrostatic model.

The electrical data taken together with the structural organization of the mucosal surface suggest a model consisting of a large set of parallel coplanar strips each of width h_1 and separated from each other by the distance h_2. The strips are charged alternatingly to the potentials $+U_0$ and $-U_0$ volts. In the following, we shall evaluate only the potential distribution produced by two coplanar strips. The lengths of the strips are assumed to be much greater than the widths h_1 and h_2, i.e., the potential distribution is invariant along any line which is parallel to the direction of the strips. Thus, the mathematical problem is reduced to that of finding a two-dimensional potential distribution $U(x, y)$.

Cartesian coordinates (x, y, z) are used as the reference system. The plane surface containing the two coplanar strips is placed in the (x, z)-plane with the strips directed parallel to the z-axis and placed symmetrically with respect to the origin, the boundaries of the strips on the x-axis being at $\pm x_0$ and $\pm x_1$, i.e., the width h_1 above is equal to $x_1 - x_0$, and $2x_0$ equals the distance h_2 between the strips. The potential profile $U(x, y)$ must satisfy Laplace's equation in the upper half-plane, i.e.,

$$\frac{\partial^2 U}{\partial x^2} + \frac{\partial^2 U}{\partial y^2} = 0, \quad \text{for } -\infty \leq x \leq \infty \quad \text{and} \quad 0 \leq y \leq \infty \tag{A1}$$

and $U(x,y)$ must conform to the two boundary conditions

$$U(x, y) \to 0, \quad \text{for } x \to \pm\infty \quad \text{and} \quad y \to \infty \tag{A2}$$

and

$$U(x, 0) = F(x) = \begin{cases} -U_0 & \text{for } -x_1 \le x \le -x_0 \\ +U_0 & \text{for } x_0 \le x \le x_1 \\ 0 & \text{elsewhere} \end{cases} \quad \text{(A3)}$$

on the x-axis. Thus $U(x, y)$ belongs to the class of functions which is harmonic in the upper half-space and takes the definite value $U(x, 0) = F(x)$ on the x-axis (the half-plane problem). These functions have as a general solution an integral formula of the Poisson type (*see*, e.g., Churchill, 1960; Morse & Feshbach, 1953)

$$U(x, y) = \frac{y}{\pi}\int_{-\infty}^{+\infty} \frac{F(\lambda)}{y^2 + (\lambda - x)^2}\, d\lambda \quad \text{(A4)}$$

or

$$U(x, y) = \frac{y}{\pi}\int_0^{\infty} F(\lambda)\left\{\frac{1}{y^2 + (\lambda - x)^2} - \frac{1}{y^2 + (\lambda + x)^2}\right\} d\lambda \quad \text{(A5)}$$

if $F(\lambda)$ is odd as in Eq. (A3). Inserting this value for $F(\lambda)$ into Eq. (A5) gives

$$U(x, y) = \frac{yU_0}{\pi}\int_{x_0}^{x_1} \frac{d\lambda}{y^2 + (\lambda - x)^2} - \frac{yU_0}{\pi}\int_{x_0}^{x_1} \frac{d\lambda}{y^2 + (\lambda + x)^2}. \quad \text{(A6)}$$

The evaluation of these integrals results in a solution of the above boundary value problem in the form

$$U(x, y) = \frac{U_0}{\pi}\arctan\left\{\frac{2xy}{y^2 + x_0^2 - x^2}\right\} + s_1 U_0 - \frac{U_0}{\pi}\arctan\left\{\frac{2xy}{y^2 + x_1^2 - x^2}\right\} - s_2 U_0 \quad \text{(A7)}$$

where the two discontinuous factors s_1 and s_2

$$s_1 = \begin{cases} 0, & \text{for } y^2 + x_0^2 - x^2 \ge 0 \\ 1, & \text{for } y^2 + x_0^2 - x^2 < 0 \end{cases}$$

and

$$s_2 = \begin{cases} 0, & \text{for } y^2 + x_1^2 - x^2 \ge 0 \\ 1, & \text{for } y^2 + x_1^2 - x^2 < 0 \end{cases} \quad \text{(A8)}$$

eliminate the discontinuity $(\infty, -\infty)$ in the argument ν of arctan ν which occurs when the denominator in the expressions inside the { } in Eq. (A7) takes the values $0 + \varepsilon$ and $0 - \varepsilon$ where $\varepsilon \ll 0$.

The distribution of the flux or current lines $V(x, y)$ have the properties:

(*i*) $V(x, y)$ is harmonic in the upper half-plane like the potential distribution $U(x, y)$, and (*ii*) each flux line is orthogonal to every equipotential line in the upper half-plane.

Since we are dealing with a two-dimensional problem, the most convenient way to determine the function $V(x, y)$ is to use the theory of complex variables and consider the function

$$W(\zeta) = U(\xi, \eta) + \iota V(\xi, \eta) \quad \text{(A9)}$$

where $\iota = \sqrt{-1}$ and $\zeta = \xi + \iota\eta$ is a point in the complex number plane (ξ, η). The function $W(\zeta)$ is assumed to be analytic. The functions U and V will then satisfy the Cauchy-Riemann conditions, i.e.,

$$\frac{\partial U}{\partial \xi} = \frac{\partial V}{\partial \eta} \quad \text{and} \quad \frac{\partial U}{\partial \eta} = -\frac{\partial V}{\partial \xi}. \quad \text{(A10)}$$

This is the condition for the functions $U(\xi, \eta)$ and $V(\xi, \eta)$ to be harmonic conjugates, and also that the family of curves $U(\xi, \eta)$ = constant and $V(\xi, \eta)$ = constant intersect each other orthogonally. Thus, if we choose the set $U(\xi, \eta)$ to represent the equipotentials—and the functional dependence being given by Eq. (A7)—then $V(\xi, \eta)$ represents the corresponding lines of force or current lines. If $U(\xi, \eta)$ is known one can find its harmonic conjugate $V(\xi, \eta)$ by integration of the total differential of V

$$dV = \left(\frac{\partial V}{\partial \xi}\right) d\xi + \left(\frac{\partial V}{\partial \eta}\right) d\eta = -\left(\frac{\partial U}{\partial \eta}\right) d\xi + \left(\frac{\partial U}{\partial \eta}\right) d\eta \quad \text{(A11)}$$

because the Cauchy-Riemann conditions make the right-hand side known functionally. This standard procedure turned out to be rather tedious with the functional dependence of $U(x, y)$ given by Eq. (A7). Instead we used another result from the theory of complex variables which is related to the method shown by Eq. (A4) to find the formula for $U(x, y)$: Let $U(\xi, \eta)$ and $V(\xi, \eta)$ be the complex conjugates of the analytic complex function $W(\zeta)$, where $\zeta = \xi + \iota\eta$. If the values of $U(x, y)$ in the point $z = x + \iota y$ are given by Poisson's integral formula for a plane

$$U(x, y) = \frac{y}{\pi}\int_{-\infty}^{+\infty} \frac{F(\xi)}{(x - \xi)^2 + y^2}\, d\xi \quad \text{(A12)}$$

where the values of $U(\xi, \eta)$ on the real axis ξ are given by $U(\xi, 0) = F(\xi)$, then the value of the harmonic conjugate $V(x, y)$ in the same point can be shown to be given by

$$V(x, y) = \frac{1}{\pi}\int_{-\infty}^{+\infty} \frac{(x - \xi)F(\xi)}{(x - \xi)^2 + y^2}\, d\xi \quad \text{(A13)}$$

(*see*, e.g., Churchill, 1960; Morse & Feshbach, 1953). Inserting Eq. (A3) into Eq. (A13) gives

$$V(x, y) = -\frac{U_0}{\pi}\int_{-x_1}^{-x_0} \frac{(x - \xi)F(\xi)}{(x - \xi)^2 + y^2}\, d\xi + \frac{U_0}{\pi}\int_{x_0}^{x_1} \frac{(x - \xi)F(\xi)}{(x - \xi)^2 + y^2}\, d\xi = \frac{1}{2\pi}\ln\left\{\frac{(x_0 - x)^2 + y^2}{(x_1 - x)^2 + y^2} \cdot \frac{(x_0 + x)^2 + y^2}{(x_1 + x)^2 + y^2}\right\}. \quad \text{(A14)}$$

The family of curves $U(x, y)$ = constant and $V(x, y)$ = constant were obtained by developing a Fortran program which would find from Eq. (A7) the contour lines for $U(x, y)$ and from Eq. (A14) those of $V(x, y)$, i.e., the set of (x, y) values belonging together when either the left-hand side of Eq. (A7) was given a value $U(x, y)$ = constant or a value $V(x, y)$ = constant was assigned to the left-hand side of Eq. (A14). An example is shown in Fig. 14 using the values: $x_0 = 20$ μm, $x_1 = 120$ μm and $U_0 = 100$ μm.

If the region above the (x, y) – plane consists of a conducting material an electric current will flow along the flux lines $V(x, y)$ = constant from strip at potential $+U_0$ to the adjacent one at

potential $-U_0$. A few of these current lines are shown in Fig. 14. The current density at every point in space can be resolved into a horizontal component, I_x, and a vertical component, I_y, which are given by

$$I_x(x, y) = -\frac{1}{\rho}\frac{\partial U}{\partial x} \quad \text{and} \quad I_y(x, y) = -\frac{1}{\rho}\frac{\partial U}{\partial y} \tag{A15}$$

where ρ is the resistivity of the medium. To obtain the vertical component of the current density of the model we invoke Eq. (A14) into the above right-hand equation. This gives

$$I_y(x, y) = \frac{1}{\rho}\frac{U_0}{\pi} 2x \frac{[y^2 + x_0^2 - x^2] - 2y^2}{[y^2 + x_0^2 - x^2]^2 + 4x^2y^2}$$

$$- \frac{1}{\rho}\frac{U_0}{\pi} 2x \frac{[y^2 + x_1^2 - x^2] - 2y^2}{[y^2 + x_1^2 - x^2]^2 + 4x^2y^2}. \tag{A16}$$

In Fig. 15 are shown vertical current densities $I_y(x, y)$, together with the potential profiles according to Eq. (A7), calculated at the two positions $x = 60$ μm and $x = 80$ μm and using the experimental values $\rho = 56\ \Omega \cdot$ cm, and the average value for the surface potential $U_0 = 45$ μV.